AGU PUBLICATIONS

Tectonics

RESEARCH ARTICLE
10.1002/2016TC004459

Key Points:
- Unfolding and hinge migration occurred during inversion of the sedimentary basin
- Paleomagnetic data can be used as a continuous kinematic indicator for palinspastic reconstructions
- Reliable paleomagnetic direction (350 and 53) for Albian times in Iberia

Correspondence to:
C. García-Lasanta,
cgarcialasanta@gmail.com

Citation:
García-Lasanta, C., A. Casas-Sainz, J. J. Villalaín, B. Oliva-Urcia, T. Mochales, and F. Speranza (2017), Remagnetizations used to unravel large-scale fold kinematics: A case study in the Cameros Basin (Northern Spain), *Tectonics*, *36*, doi:10.1002/2016TC004459.

Received 3 JAN 2017
Accepted 3 APR 2017
Accepted article online 6 APR 2017

Remagnetizations used to unravel large-scale fold kinematics: A case study in the Cameros Basin (Northern Spain)

C. García-Lasanta[1], A. Casas-Sainz[1,2], J. J. Villalaín[3], B. Oliva-Urcia[4], T. Mochales[5], and F. Speranza[6]

[1]Earth Sciences Department, Universidad de Zaragoza, Zaragoza, Spain, [2]Geotransfer (Instituto Universitario de Ciencias Ambientales), Universidad de Zaragoza, Zaragoza, Spain, [3]Physics Department, Universidad de Burgos, Burgos, Spain, [4]Geology and Geochemistry Department, Universidad Autónoma de Madrid, Madrid, Spain, [5]Instituto Geológico y Minero de España, Madrid, Spain, [6]Istituto Nazionale di Geofisica e Vulcanologia, Rome, Italy

Abstract The occurrence of a generalized remagnetization at 100 Ma makes the Cameros Basin, an 8 km thick Cretaceous extensional trough inverted during the Cenozoic, a perfect natural frame to apply paleomagnetic vectors to geometrical reconstructions. The widespread remagnetization that occurred between the extensional and compressional episodes, linked to low-grade metamorphism, provides a tool to reconstruct the attitude of beds at the remagnetization time, thus giving a picture of basin geometry during the Cretaceous. This snapshot is compared with the present-day geometry to constrain the large-scale kinematic evolution of folds between these two stages. According to this methodology, a syncline, preinversion geometry of the sedimentary basin was determined and the position of its main axial surface was accurately located. Comparing with the present-day, postinversion geometry, a northward hinge migration of around 5 km is inferred. This migration is the result of the southward back thrusting in the southern basin border, favored by the detachment level at the base of the Mesozoic cover. Conversely, the main northward directed thrust, which involved both the Paleozoic basement and the Mesozoic cover, did not significantly affect the internal structure of the basin in spite of its overall displacement of more than 20 km.

Plain Language Summary The Cameros basin (N Spain) developed during the Mesozoic and was inverted during the Alpine orogeny (Cenozoic). The generalized remagnetization undergone by its rocks and dated at 100 M.a. (between the extensional and the compressional stages) makes the basin a perfect natural frame to apply paleomagnetic vectors to geometrical reconstructions. By restoring the obtained remagnetized vectors to their position during the remagnetizing event together with the beds containing them, we were able to describe the geometry of the basin before the Cenozoic compression. According to the new data provided here, a syncline geometry of the sedimentary basin can be determined and the position of its main axial surface can be accurately located. In comparison with the present-day geometry (post-inversion attitude), a northwards hinge migration of around 5 km can be interpreted.

1. Introduction

Hinge migration is a frequent deformational process in fold-and-thrust belts. This mechanism is implicit in the evolution of fault-bend and fold-propagation folds [e.g., *Jamison*, 1987; *Mitra*, 1990; *Suppe*, 1983; *Mueller and Suppe*, 1997], linked to transport of the hanging-wall strata along the footwall ramps (Figure 1). However, conventional kinematic indicators witnessing this migration are rarely preserved and continuous markers are needed to face the problem in a proper way [e.g., *Mercier et al*., 2007, and references therein]. The lack of unequivocal indicators related to the basinal stage, such as growth strata geometries and the ambiguous structural features, hampers to accurately document large-scale hinge migrations involving the whole sedimentary pile [*Mercier et al*., 2007]. Consequently, defining mechanism of hinge migration during basin inversion is still a matter of debate. This is mostly because the characterization of the geometry of extensional sedimentary basins that underwent a subsequent tectonic inversion is usually problematic due to the strong modifications that the latter may imprint in the original basin geometry [e.g., *Buchanan and McClay*, 1991; *McClay*, 1989, 1995].

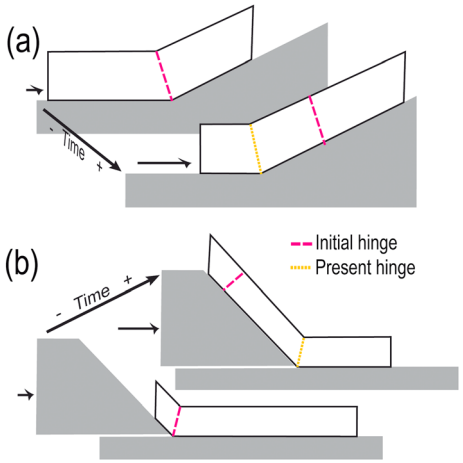

Figure 1. Block diagrams for the evolution of cover thrust sheets linked to hinge migration [modified from *Mercier et al*., 2007]. (a) Relative hinge migration as a result of fault-bend folding. (b) Hinge migration as a result of basement thrusting.

Paleomagnetism constitutes a valuable kinematic indicator whose utility in tectonic studies has been validated during the last decades [e.g., *McClelland et al*., 1986; *Van der Voo*, 1990; *Butler*, 1992; *McCaig and McClelland*, 1992; *Tauxe*, 1998]. It can be used to detect tectonic deformations, interpreted as modifications in the original paleomagnetic directions due to vertical axes rotations [e.g., *Van der Voo*, 1993; *Weil and Sussman*, 2004]. More recently, paleomagnetism has revealed its potential as a tool to record horizontal axes rotation in inversion tectonic contexts in the reconstruction of folds and basin geometries [e.g., *Watson and Enkin*, 1993; *Villalaín et al*., 2003, 2015; *Henry et al*., 2004; *Soto et al*., 2008, 2011; *Casas et al*., 2009]. These studies establish the conditions under which the use of paleomagnetism is appropriated to infer the kinematics of basin development and to evaluate how a remagnetization process recorded in a relatively short period can be used to picture a snapshot in basin evolution. Remagnetizations are relatively common in sedimentary basins because they are linked to frequent processes of basin evolution [*Elmore et al*., 2012, and references therein], such as fluid circulation [e.g., *Van der Voo and Torsvik*, 2012, and references therein], illite-smectite transformations [e.g., *Katz et al*., 1998; *Tohver et al*., 2008], organic matter maturation [e.g., *Blumstein et al*., 2004], and other mechanisms associated to sedimentary burial [e.g., *Banerjee et al*., 1997; *Katz et al*., 1998; *Villalaín et al*., 2003; *Aubourg et al*., 2012].

The geological unit studied in this work is the Cameros Massif (Figure 2a). It shows several of the features where paleomagnetism can represent a valid tool to interpret its tectonic background. The widespread remagnetization documented in the basin is a first-order feature that allows, at large scale, to accurately identify the geometrical change of the Cameros unit between its basinal and inverted stages. Therefore, it provides an insight in the occurrence of unfolding and hinge migration processes. In particular, the interest of deciphering hinge migration in this context lies in (i) the regional, plurikilometric scale of the described structures and (ii) the novelty of using paleomagnetic vectors as specific markers of tectonic deformation that provides the methodological dimension to this study.

2. Geological Context

The Cameros Basin constitutes the westernmost and most subsiding basin of the whole extensional system developed in the Iberian Range (Northern Spain) during the Early Cretaceous (Figures 2a and 2b). This extensional system, triggered by the spreading of the North Atlantic Ocean, developed its rifting stage in the Iberian Domain as intraplate, relatively small sized basins [e.g., *Ziegler*, 1988].

NW-SE oriented normal faults controlled the extensional process in the Cameros Basin [e.g., *Guiraud*, 1983; *Gil Imaz*, 2001] during the Early Cretaceous. Continental sediment thickness reached up to 8000 m during the Tithonian and Albian extensional tectonics [*Casas et al*., 2009] (Figure 2c). These sediments were deposited in fluvial to lacustrine environments along time and are divided into five lithostratigraphic units from bottom to top: Tera, Oncala, Urbión, Enciso, and Oliván Groups [*Tischer*, 1966]. Extension and normal faulting of the basement yielded bending of the sedimentary cover, where normal faults and tension gashes developed, more frequently in the lower units. Extension reached its maximum during the Albian, coeval with the deposition of the Oliván Group [e.g., *Casas-Sainz and Gil-Imaz*, 1998; *Mata et al*., 2001]. Bending produced a gentle large-scale syncline geometry of the sedimentary pile [*Casas et al*., 2009]. During an intermediate stage, probably Albian in age, penetrative axial-plane cleavage was generated in the synextensional rocks from the

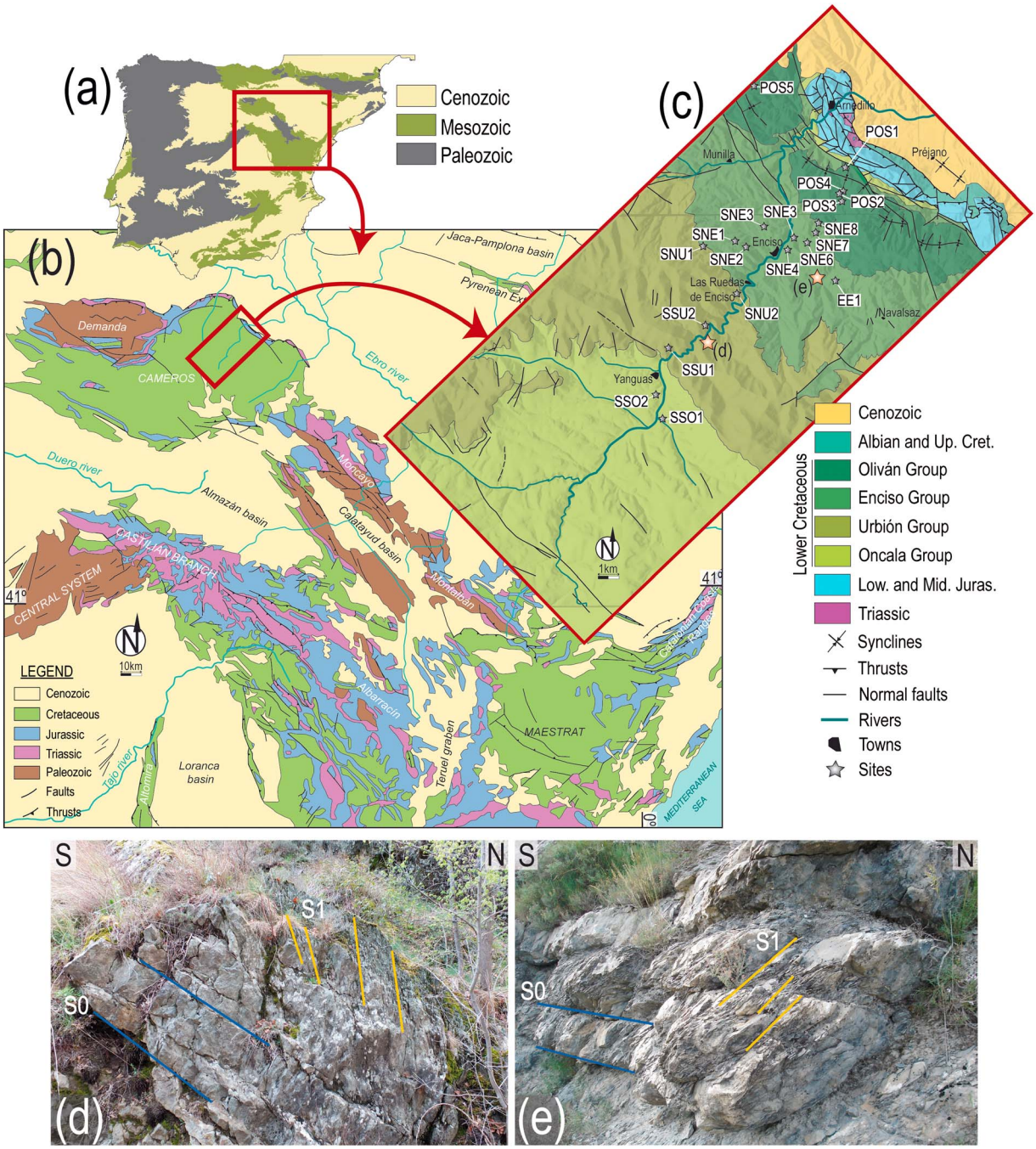

Figure 2. (a) Location of the Iberian range within the Iberian Peninsula. (b) Geological sketch of the Iberian Range and location of the studied region. (c) Geological map of the Cidacos Valley and surrounding area, together with the location of the paleomagnetic sites sampled for the study (modified from Cartografía Geológica Digital Continua a Escala 1:50.000 [*GEODE*, 2014]). (d) Outcrop in southern flank of the Cameros Syncline showing bedding and a steeply northward dipping cleavage (see map in Figure 2c for location). (e) Outcrop in southern flank of the Cameros Syncline showing north dipping beds and southward dipping cleavage (see map in Figure 2c for location).

Jurassic limestones up to the lower part of the Oliván Group [*Gil Imaz*, 2001]. The spatial distribution of this cleavage is associated with specific lithologies, being pervasive in siltstones and marls, and scarce in massive and more competent materials [*Gil Imaz*, 2001]. Subsequently, a low-grade metamorphism episode dated at around 100 Ma [*Casquet et al.*, 1992] affected the synextensional deposits [*Guiraud and Séguret*, 1985; *Goldberg et al.*, 1988; *Mata et al.*, 2001], yielding lower metamorphic degree conditions moving away from the basin depocenter [*Mata*, 1997; *Del Río et al.*, 2009]. The work by *Villalaín et al.*

[2003] links this metamorphic peak to the general remagnetization of the Lower Cretaceous series that occurred during the Albian stage.

Cenozoic Alpine compression caused the complete tectonic inversion of the basin [*Guimerà and Álvaro*, 1990; *Casas-Sainz and Faccenna*, 2001]. A northward basin transport occurred along a large-scale system of basement thrusts channelized toward the surface in the Upper Triassic Keuper facies. The synextensional series moved northward, thrusting over the molasse of the Cenozoic Ebro Basin in the Cameros foreland (Figures 2b and 2c). The thrusting direction is approximately coaxial with the extensional direction [e.g., *Casas-Sainz and Gil-Imaz*, 1998]. This late episode produced the complete exhumation of the synextensional series, forming at present a monotonous northward dipping monocline except in the northern basin border [e.g., *Casas-Sainz*, 1991]. This border is at present defined by a hanging-wall, kilometric-scale syncline (Northern Cameros Syncline), whose northern flank is strongly thinned with respect to its southern flank.

Two geometrical relationships between cleavage and bedding are observed in different parts of the large monocline [*Casas-Sainz and Gil-Imaz*, 1998]: in the south, north dipping bedding and steeper cleavage are observed (Figure 2d). Conversely, in the northern part of the monocline (i.e., bedding still dipping north), south dipping cleavage planes, with subhoriztonal to 45°S dips are observed (Figure 2e). As flexural-flow mechanism for cleavage formation is assumed [*Casas-Sainz and Gil-Imaz*, 1998; *Gil Imaz*, 2001], the two areas of the same monocline should correspond to different limbs of a previous syncline. Therefore, an unfolding process must be involved in its evolution.

3. Aim of the Study and Sampling Design

In this work, we focus on the central eastern sector of the Cameros Basin (Cidacos Valley) in order to disentangle the kinematics of basin inversion by a detailed paleomagnetic study. The set of samples includes sites from the Oncala, Urbión, Enciso, and Oliván Groups and allows to characterize the remagnetization effects on different lithologies and positions within the sedimentary pile. All sites are distributed along a single NE-SW profile, and consequently, they can be plotted along a cross section perpendicular to the main structural attitude. The 20 paleomagnetic sampled sites are distributed as follows (Figure 2c): (i) two sites were sampled in dark grey, fine marly limestones from the Oncala Group; (ii) four sites were gathered in the Urbión Group, with lithologies varying from multicolored shales to brown clayey siltstones; (iii) nine sites were collected in the Enciso Group, including two sites in red clayey siltstones and seven sites in grey limestones and marly limestones; and finally, (iv) five sites were sampled in the Oliván Group, in reddish siltstones. The anisotropy of magnetic susceptibility results from sites in Oncala and Urbión, and three sites from the Enciso Group were shown by *García-Lasanta et al*. [2014]. Cleavage attitude in north dipping beds of the Enciso Group suggests the probable location of the Mesozoic axial surface in this area and thus justifies the special emphasis on its sampling.

Most samples were collected in sites showing NE dipping strata, except for the Oliván Group sites that are often deflected from this trend and show anomalous tilts associated with the Cameros thrust front [*Casas-Sainz et al*., 2016]. This is probably related to an accommodation of strata over the footwall ramp during the Cenozoic inversion. Bedding orientations of the 20 outcrops are slightly different from the general data set presented by *Villalaín et al*. [2003] in other areas of the Cameros unit, where the general strike of beds was around E-W. This difference provides the opportunity to add our paleomagnetic results to that previous data set and to recalculate the orientation of the theoretical paleomagnetic vector for the Cameros Basin during the Cretaceous, by means of the small circles intersection (SCI) method [*Shipunov*, 1997; *Waldhör and Appel*, 2006]. Since *Villalaín et al*. [2003] bracketed the remagnetization in the Cameros domain between the rift and inversion stages, it is possible to reconstruct the attitude of bedding at the preinversion stage with the SCI method. *Villalaín et al*. [2015] proposed a technique for a partial restoration of the paleomagnetic vectors (i.e., *asymmetric solution*) that consists in restoring each vector to the expected direction at the remagnetization time. As an exact rotation value is given for the strata containing each vector, the method allows restoring strata attitude at the remagnetization time.

4. Methods

The natural remanent magnetization (NRM) carriers were determined by rock magnetism techniques. Several curves of acquisition of the isothermal remanent magnetization (IRM) were obtained from powdered samples

representing all the studied lithologies by applying increasing magnetic fields and measuring the remanent magnetization in each step, up to 1 T. Backfield was also applied stepwise until magnetic remanence was completely erased. Curves registering induced magnetization variations under increasing and decreasing temperatures (thermomagnetic curves) were also obtained from the same samples in the translation balance. Hysteresis loops were also performed by inducing progressively higher magnetic fields, up to 1 T, and, subsequently, decreasing fields in the opposite sense. All previous data were obtained using a Magnetic Measurements Variable Field Translation Balance in the Paleomagnetic Laboratory of the University of Burgos (Spain). Complementary to these techniques, the thermal demagnetizations of a composite IRM [*Lowrie*, 1990] were done at the Laboratory of Paleomagnetism of Istituto Nazionale di Geofisica e Vulcanologia (INGV) (Rome, Italy). This procedure allows the identification of ferromagnetic minerals based on both their coercivities and unblocking temperatures spectra. It consists of thermal demagnetizing samples which were previously magnetized at 2000, 500, and 120 mT along the *z*, *y*, and *x* sample axes, respectively.

A total set of 220 standard samples from the 20 sites was subjected to thermal demagnetization in the paleomagnetic laboratories of the INGV and the University of Burgos. Results from the magnetic mineralogy experiments helped to design two demagnetization strategies, depending on the magnetic phases detected in each lithology. Stepwise thermal demagnetization was applied (i) in 15 temperature steps up to 540°C, to samples in which no hematite was expected, and (ii) in 14 steps up to 680°C to reddish samples with probable presence of hematite where a high coercive fraction was previously detected by rock magnetic analyses. Heating cycles were developed in an ASC TD48 oven, in absence of magnetic field, and the remanent magnetization was measured by a cryogenic magnetometer (2G Enterprises, USA). Magnetic susceptibility was measured with a KLY-2 and KLY-4 susceptometers (AGICO) in order to control mineral neoformation during heating. Demagnetization behaviors were checked by plotting results in orthogonal vector diagrams [*Zijderveld*, 1967]. The characteristic component in each sample was assessed visually and calculated by linear regression using Remasoft 3.0 software [*Chadima and Hrouda*, 2006]. Site mean directions were calculated by Fisher's statistics [*Fisher*, 1953]. A regional fold test was performed to all 20 sites using the PmagPy software by *Tauxe* [2010], in order to assess the "synfolding" remagnetization characteristics.

The small circles intersection (SCI) method [*Shipunov*, 1997; *Waldhör and Appel*, 2006] was applied in order to obtain the most probable direction for the syntectonic remagnetization. This method uses the mean paleomagnetic direction together with the strike of the beds at each site. The magnetization vector rotates together with the bed around a horizontal axis parallel to bedding strike. The vector follows a small circle trajectory according to that direction at a constant angle with the rotation axis. The small circle represents all remagnetization direction during rotation. In principle the remagnetization could have been acquired at any stage of folding development, so all directions defined by a small circle must be considered. In this sense, the intersection of the different small circles (from each site in which a remagnetized vector could be obtained) defines the most probable direction for the remagnetization at the acquisition time. This solution of the SCI method is calculated as the direction that minimizes the parameter $A = \Sigma|\alpha_i|$, where α_i are the angular distance between the mentioned direction and the small circles, *i* [*Waldhör and Appel*, 2006]. For syntectonic remagnetization, the restitution of paleomagnetic direction for each site is in general unknown. For the directions restitution we apply the asymmetric solution method [*Villalaín et al*., 2003, 2015] in order to obtain the attitude of beds at the remagnetization time. The remagnetized vector is rotated (together with its corresponding bedding plane) to the expected remagnetization direction. The expected direction can be obtained from the apparent polar wander path, whenever it and the age of the overprint are well constrained. Otherwise, the result of the SCI method is a very good estimation of the remagnetization direction. This allowed us to obtain the beds paleodip at the remagnetization time.

5. Results

5.1. Carriers of the NRM

Results from rock magnetic analyses demonstrate the presence of different ferromagnetic minerals related to sample lithology (Figure 3). The IRM acquisition curves show strong magnetic remanence in red, brown, and multicolored siltstones and shales (samples SNE2-7 and SSU2–7 in Figure 3). In these samples, well-defined IRM curves do not register a complete magnetic saturation when reaching 1 T and back-field values

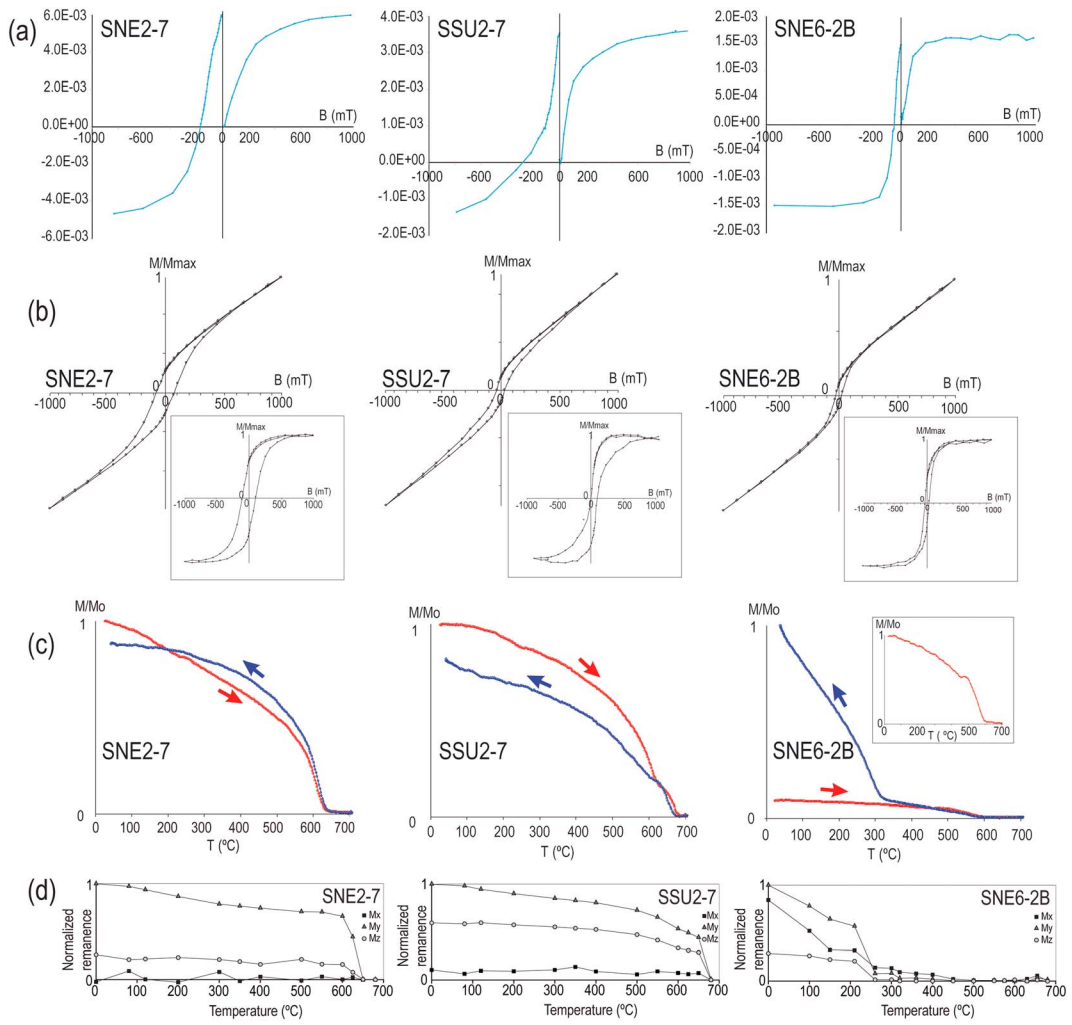

Figure 3. Rock magnetism results from three representative samples: (a) IRM acquisition curves and backfield, (b) hysteresis loops (paramagnetic effect subtracted in the right, smaller graphics), (c) magnetization versus temperature curves, and (d) thermal demagnetization of composite IRM.

are higher than in samples without hematite (Figure 3a). Hysteresis loops confirm the presence of ferromagnetic minerals, according to the separation of the two halves of each loop on the highest applied field segments (Figure 3b). Magnetization decays at temperatures above 620°C (Figure 3c). Such evidence points to the occurrence of hematite in these reddish samples (Figure 3c). Likewise, thermal demagnetizations of composite IRM confirm the presence of a high coercive phase (high magnetization values observed at high and intermediate fields), and its demagnetization occurs at temperatures above 640°C, as expected for hematite (Figure 3d).

Grey and dark grey limestones and shales present lower intensities than red shales (sample SNE6-2B in Figure 3), probably due to their smaller ferromagnetic fraction occurrence. In any case, the IRM curves show a complete saturation and the back-field value is much lower than the one measured in the hematitic samples (Figure 3a), pointing to the presence of low coercivity ferromagnetic minerals (Figure 3b). This is confirmed by their hysteresis loops. The low coercivity mineral is identified as magnetite according to the magnetization decay observed in the heating thermomagnetic curves at around 580°C (Figure 3c). In the thermal demagnetization of composite IRM, a small content of magnetite can be identified when observing separately the signal decay along the low field axis, Mx, above 450°C (Figure 3d). This test also shows the presence of an intermediate coercive phase whose demagnetization temperature matches with the temperature expected for pyrrhotite (between 260°C and 325°C).

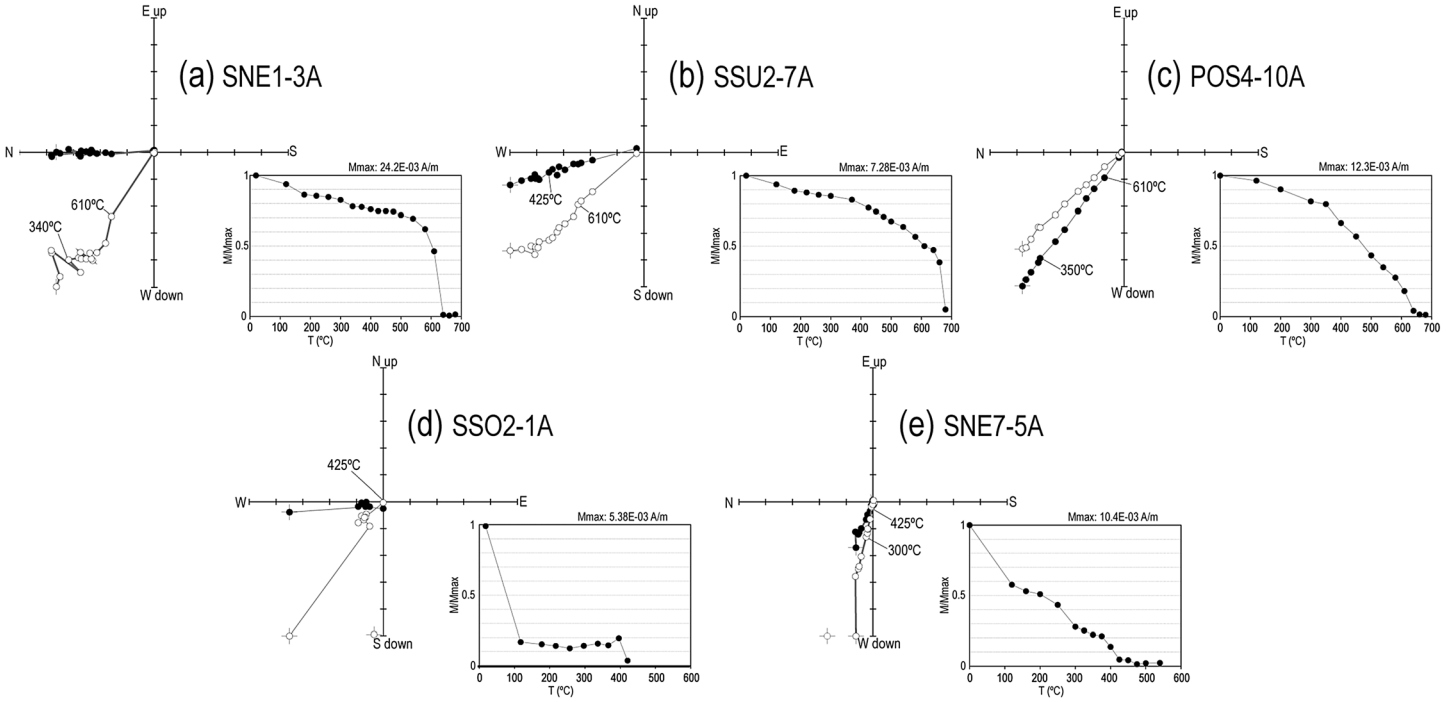

Figure 4. (a–e) Representative NRM thermal demagnetizations of samples from the study. All directions in Zijderveld diagrams are plotted before tectonic correction. Normalized intensity of the NRM (M/Mmax) is also included.

5.2. Paleomagnetic Behavior

Results from thermal demagnetizations also point to the presence of two types of samples, according to the NRM intensity and to the ranges of unblocking temperatures. In a first set of sites (red shales and small grain-sized siltstones from Urbión, Enciso, and Oliván Groups) magnetization is mostly carried by hematite. Some of these samples maintain their magnetization at around 620–640°C (Figure 4a) or higher temperatures (Figure 4b), and from that point on, complete demagnetization occurs abruptly. Other samples from this set undergo a gradual demagnetization from 400°C, but, likewise, they are not completely demagnetized until 660–680°C (Figure 4c).

A second set of sites (grey and dark grey limestones and marly limestones from Oncala and Enciso Groups) includes samples that reach a complete demagnetization at around 500°C. The two sites from the Oncala Group show a magnetic signal with very low intensity (Figure 4d). Sites from the Enciso Group belonging to this set show two segments with different slope in the demagnetization diagram (Figure 4e). The first decay occurs at around 300°C and the second and final decay at 500°C.

Regardless of these differences, the calculation of paleomagnetic components indicates homogeneous behaviors. After having removed the viscous magnetization, the characteristic remanent magnetization (ChRM) describes one single, stable component with normal polarity. The ChRM could be isolated in the demagnetization cycles of 198 specimens (Figure 5 and Table 1).

5.3. Stability Tests

The isolated component systematically shows a normal polarity. Moreover, no remarkable difference in site mean directions clustering is observed before and after tectonic correction (BTC and ATC, respectively; Figure 5b), and the same occurs when comparing data at sample scale (Figure 5).

Results of the regional fold test (considering the average components from the 20 studied sites) reveal a negative result, with a range of confidence between −29 and 60% of unfolding (Figure 5c). This result confirms the occurrence of a secondary magnetization. In addition, results point to a synfolding or postfolding origin of the characteristic component but do not give conclusive results because of the wide interval of unfolding percentage obtained.

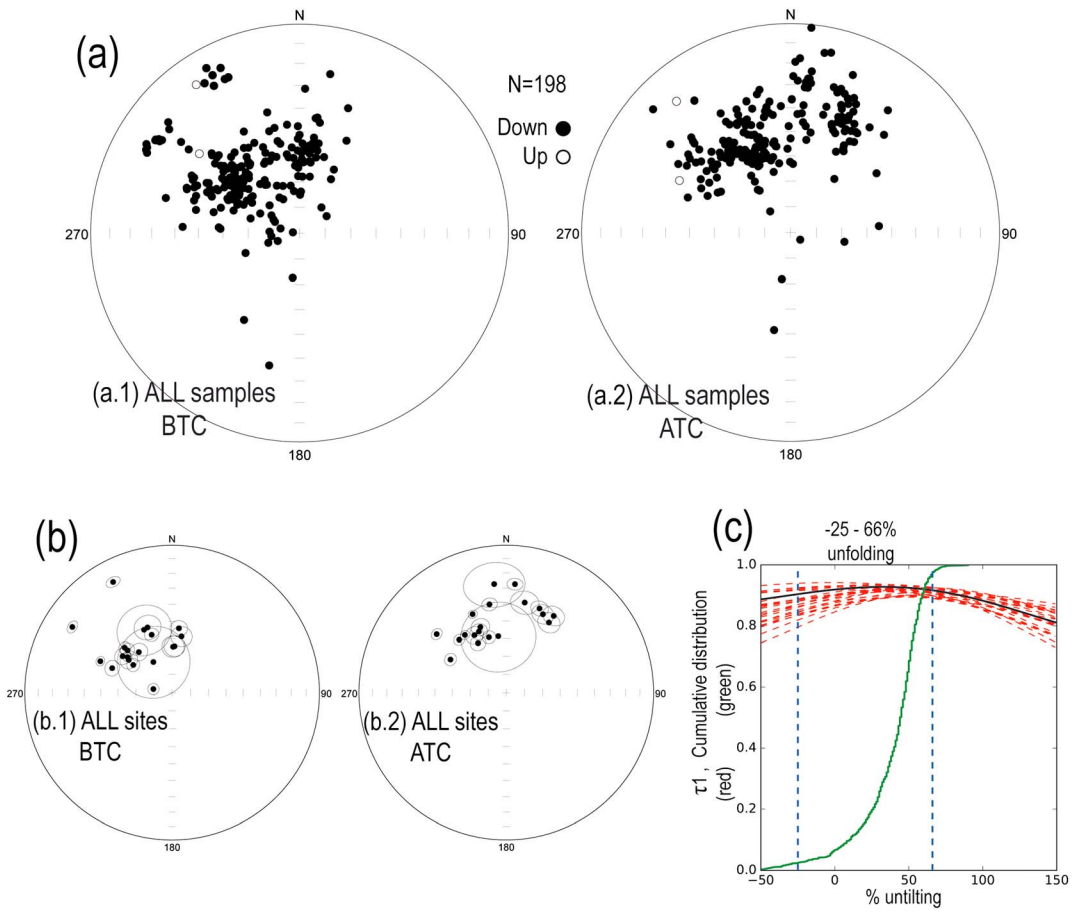

Figure 5. (a) Equal area projection of the paleomagnetic component obtained from all the samples, represented before (a.1) and after (a.2) tectonic correction. (b) Equal area projection of sites mean values BTC (b.1) and ATC (b.2), together with their 95% confidence circles. (c) Fold test at the regional scale of all the components. Eigenvalues $\tau 1$ of the orientation matrices from representative paradata sets obtained from in situ coordinates of the components versus the estimated percentage of unfolding.

5.4. Recalculation of the Expected Paleomagnetic Direction

The paleomagnetic component isolated in our samples coincides with the obtained by *Villalaín et al*. [2003], who described the results from 23 sites (about 200 samples) of red beds (siltstones and shales) from the Oncala, Enciso, and Oliván Groups. Sites were distributed in three transects perpendicular to the present-day northern basin border, west of the area studied in the present paper. These data helped *Casas et al*. [2009] to determine the expected direction of the remagnetized vector by applying the SCI method [see *Waldhör and Appel*, 2006]. However, it has been demonstrated that the structural characteristics of an area may partially influence the theoretical solution obtained from the SCI method [*Villalaín et al*., 2015]. A variety of bedding strikes are necessary in order to achieve reliable intersections between the considered small circles. Therefore, the limitation of the structural characteristics of an area limitation can be overcome by increasing as much as possible the amount of available data and their heterogeneity in terms of structural orientation [*Henry et al*., 2004; *Torres-López et al*., 2014; *Villalaín et al*., 2015]. Thus, we provide the theoretical direction of the remagnetized vector using the new set of sites together with the sites collected in the northern Cameros Basin border by *Villalaín et al*. [2003] and *Casas et al*. [2009] (Figure 6a). The SCI result obtained from these 42 sites is as follows: Dec. = 350.4° and Inc. = 53.2° (Figure 6b).

Furthermore, we have attempted to calculate an expected paleomagnetic direction from published poles for Iberia with an Albian-Cenomanian age. Six poles have been used with ages comprised between 80 and 112 Ma: Sintra granites [*Van der Voo*, 1969], Paço d'Ilhas sill [*Neres et al*., 2012], gabbros and diorites from

Table 1. Remanent Magnetization Parameters for the Characteristic Paleomagnetic Component From Each Site[a]

Site	UTM East	UTM North	Lith Group	S0 (RHR)	n/N	NRM (mA/m)	*E* (mA/m)	*k*	α95	*D* (BTC)	*I* (BTC)	*D* (ATC)	*I* (ATC)
POS1	X564553.80	Y4670203.66	Oliván	096/54	7/10	29.130	5.820	329.71	3.3	332	16	301	54
POS2	X564168.50	Y4668582.14	Oliván	288/28	7/10	30.980	14.270	640.12	2.4	310	59	337	42
POS3	X563951.96	Y4668766.28	Oliván	305/35	9/9	30.397	1.480	173.9	3.9	313.5	55.7	349.2	39
POS4	X564011.13	Y4669200.66	Oliván	006/36	11/11	17.727	6.353	240.17	3	303.3	20.1	318.3	50.3
POS5	X561630.20	Y4675035.25	Oliván	228/43	11/11	8.138	1.754	224.66	3.1	281	79.5	310	38.3
SNE1	X558061.03	Y4666971.08	Enciso	333/29	11/11	20.718	3.931	59.61	6	1.2	64.5	31.4	43.7
SNE2	X558411.70	Y4666941.11	Enciso	320/28	10/10	25.730	8.456	73.92	5.7	3	64.2	25.1	41
SNE3	X559335.05	Y4667489.91	Enciso	333/25	9/9	1.634	1.680	265.16	3.2	313.5	53.4	348.9	54.3
EE1	X561577.47	Y4665338.28	Enciso	278/10	13/15	0.937	0.394	71.66	4.9	320.7	60.8	331	53.3
SNE4	X560936.99	Y4666991.12	Enciso	300/23	13/14	1.442	0.444	72.78	4.9	307.1	59.8	338.4	50.5
SNE5	X561089.82	Y4667356.55	Enciso	321/25	11/12	0.704	0.333	120.13	4.2	292.3	53.8	330.3	58.3
SNE6	X561797.26	Y4667324.4	Enciso	318/27	12/12	1.459	0.590	297.61	2.5	293.7	45.8	324.3	50.2
SNE7	X562097.38	Y4667668.38	Enciso	309/21	11/12	8.354	2.102	160.29	3.6	305.6	63.5	342.6	57.7
SNE8	X562213.25	Y4668112.90	Enciso	313/21	11/12	3.999	3.063	104.85	4.5	306.4	55.7	335.8	52.6
SNU1	X557051.73	Y4667097.20	Urbión	336/27	7/7	48.786	15.279	113.59	5.7	9.5	58.3	31.8	38.8
SNU2	X558900.68	Y4665030.17	Urbión	328/21	9/10	25.310	6.905	134.12	4.5	6.1	53.9	21.6	38.6
SSU1	X555243.30	Y4661664.66	Urbión	306/38	10/10	8.513	1.210	163.12	3.8	340.5	55.8	4.6	27.1
SSU2	X556949.36	Y4662631.92	Urbión	334/34	9/9	12.962	14.133	54.03	7.1	339.3	51	11.6	37.7
SSO1	X554739.03	Y4658968.62	Oncala	294/16	9/11	0.152	0.093	7.58	20	328.7	70.1	351.9	58.3
SSO2	X555006.04	Y4660213.32	Oncala	296/32	8/9	0.175	0.183	15.58	14.5	335.9	51.5	353.6	26.8

[a]UTM coordinates (all sites are located in time zone 30 T, datum: ETRS89); Lith group: lithostratigraphic group within the Lower Cretaceous sequence in the Cameros massif; n/N: number of sample directions used in the analysis versus total number of demagnetized samples; NRM: site average of the natural remanent magnetization intensity (mA/m); S0 (RHR): bedding orientation (right-hand rule); *k* and α95: Fisher statistical parameters [*Fisher*, 1953]; D: declination; I: inclination (BTC: before tectonic correction: ATC: after tectonic correction).

Sintra pluton [*Storetvedt et al.*, 1987], Foz da Fonte sill [*Neres et al.*, 2012], Lisbon area sediments [*Galdeano et al.*, 1989], and sedimentary Algarve Basin [*Moreau et al.*, 1997]. The mean direction obtained is as follows: Dec. = 354.7°, Inc. = 47.0°, and α_{95} = 8° (Figure 7b). This direction must be considered with caution because, in general, Iberian Cretaceous paleomagnetic poles show questionable reliability due to the occurrence of remagnetizations and because they have been demonstrated incompatible with Global Apparent Wander Path [*Neres et al.*, 2013]. In any case, this mean direction and the SCI solution obtained from the 42 sites from

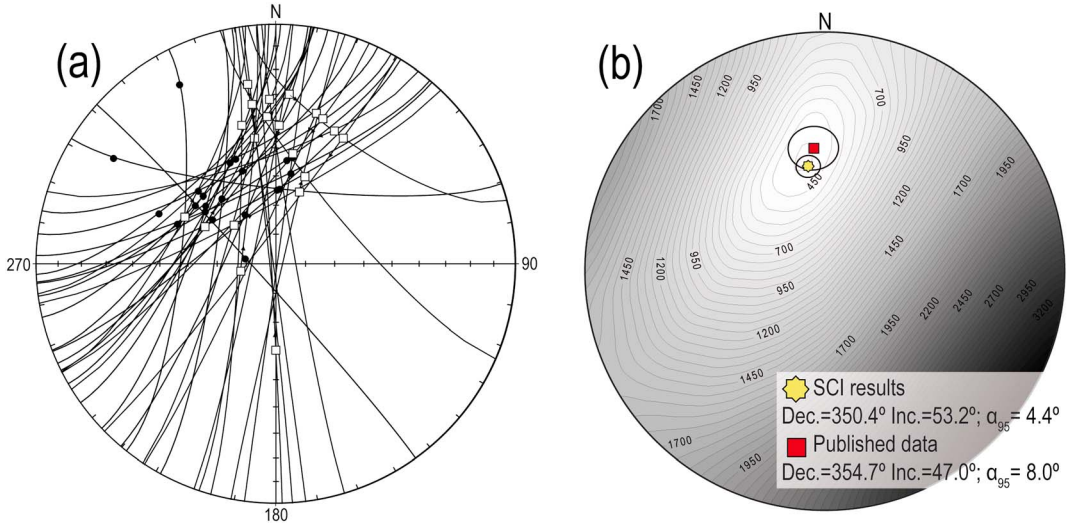

Figure 6. (a) Equal area projection of the small circles and the in situ magnetic components (i.e., before tectonic correction, BTC) of the 42 sites used for the application of the SCI method: 20 from this study (black dots) and 22 from *Casas et al.* [2009] (grey squares). (b) Equal area projection showing contours of equal value *A* [*Waldhör and Appel*, 2006], obtained from the 20 studied sites together with the 22 previous sites from *Casas et al.* [2009]. The yellow star shows the maximum value of *A* ($A = \Sigma|\alpha_i|$), and the red square shows the mean paleomagnetic direction for Albian-Cenomanian times according to published data. The 95% confidence circles are also represented.

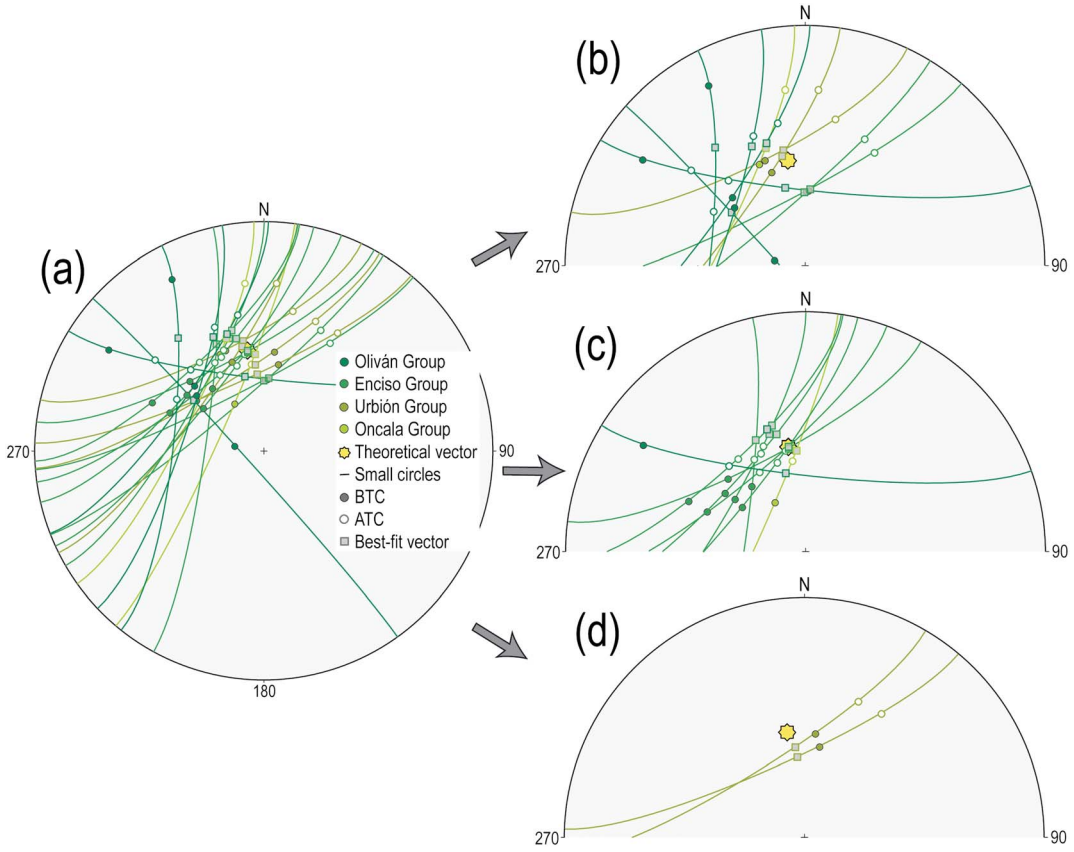

Figure 7. (a) Small circles for the obtained paleomagnetic components from all sites. Filled circles represent the in situ orientations of the paleomagnetic vectors, hollow circles represent the bedding-corrected directions of the paleomagnetic vectors, and squares represent the optimum directions of paleomagnetic vectors for each site. The star represents the expected paleomagnetic direction during remagnetization time (SCI solution). (b) Sites in which the optimum restoration is between BTC and ATC. (c) Sites in which the optimum restoration exceeds the ATC. (d) Exceptional sites in which the sense of rotation is opposite to the TC. See online version for color legend.

Cameros are statistically undistinguishable, thus reinforcing its Albian timing and its remagnetized origin. Therefore, the solution obtained from the SCI method will be used as the reference for the partial restoration of paleomagnetic vectors shown in the following section.

5.5. Best Fit Restoration

The orientation of the remanence vectors corresponding to the 20 new sites is represented in Figure 7a before and after tectonic correction (BTC and ATC, respectively). The closest orientation, within the small circle corresponding to each site, to the Albian remagnetization direction is used to obtain the rotation angle for each bedding plane [*Villalaín et al*., 2003, 2015]. Depending on the angle of restoration needed to fit each paleomagnetic vector (Figure 7a) and its behavior (according to the BTC and ATC orientations), we differentiate three groups of sites (Table 2): (i) nine sites in which the best fit vector is in an intermediate position between the ATC and BTC orientations (Figure 7b), (ii) nine sites whose restitution angle is higher than the tectonic correction (Figure 7c), and (iii) two sites that must be rotated in an opposite sense to the tectonic correction to reach the best fit paleomagnetic orientation (Figure 7d). These orientations mark the position of the paleomagnetic vectors (and consequently, of bedding) when the remagnetization event occurred.

These results can be extrapolated to obtain the attitude of strata at the remagnetization stage (Figure 8). Therefore, sites where the paleomagnetic vectors remain in an intermediate position between BTC and ATC (i) show shallower dips than BTC after restoring but maintain their present dip direction. Sites from the second group (ii) in which restitutions overtook the ATC orientation show opposite directions at the remagnetization time and at present. Sites from these two groups are relatively close to each other

Table 2. Bedding Dips at Present and at the Remagnetization Time (Paleodip), According To the Results From the Asymmetric Solution Method[a]

	Present Dip		Paleodip		
Site	Dip Direction	Dip	Dip Direction	Dip	Restit Group
POS1	186	54	186	26.2	i
POS2	108	28	108	3.6	i
POS3	35	35	35	9.9	i
POS4	96	36	276	21.3	ii
POS5	318	43	318	20.9	i
SNE1	63	29	63	27.4	i
SNE2	50	28	50	27.6	i
SNE3	63	25	243	1.4	ii
EE1	98	10	278	6.9	ii
SNE4	30	23	210	5	ii
SNE5	51	25	231	14.4	ii
SNE6	48	27	228	19.3	ii
SNE7	39	21	219	6.9	ii
SNE8	43	21	229	9.5	ii
SNU1	66	27	66	36.3	iii
SNU2	58	21	58	30.3	iii
SSU1	36	38	36	30.9	i
SSU2	64	34	64	25.8	i
SSO1	24	16	204	3.6	ii
SSO2	26	32	26	25.4	i

[a]*Restit group* refers to the classification shown in the text according to the degree of restitution gone by each site.

(Table 2 and Figures 8 and 9). The two sites from the third group (iii) show a steeper bedding dip at the remagnetization time and need further interpretations.

6. Tectonic Interpretation and Discussion

The key point to interpret the obtained results is the homogeneity and widespread imprint of the remagnetization episode. The directional analysis of demagnetizations diagrams reveals that the carrier of the remanence varies accordingly with lithology: hematite in red beds and pyrrhotite and magnetite in grey limestones/marls. The Albian remagnetization event, dated around 100 Ma (Long Normal Cretaceous Superchron), has been described not only in the Cameros Basin but also in other areas of the western Tethys, such as the High Atlas [*Torres-López et al.*, 2014], the Basque-Cantabrian Basin [*Soto et al.*, 2008, 2011], and the Maestrat Basin [*Villalaín et al.*, 2012]. These studies demonstrated that remagnetization affected the whole sedimentary pile. Particularly in the Cameros Basin, the remagnetized sediments include the grey limestones and marly limestones and the red shales and siltstones from Upper Jurassic to Lower Cretaceous levels. These works lay the foundations for interpreting a coeval remagnetization in Northern Iberia whose carriers are these two (three) main ferromagnetic phases. Therefore, it is likely that the paleomagnetic vectors shared originally the same orientation. The restoration of these paleomagnetic vectors to the expected direction gives therefore the geometrical snapshot of the basin during the Albian, before being affected by its complete tectonic inversion during the Cenozoic.

Nevertheless, the tight timing of events occurring at the end of the Early Cretaceous (end of rifting, bending, folding associated with cleavage formation, low-grade metamorphism, and remagnetization) hinders distinguishing between geometries resulting only from extensional tectonics [see *Soto et al.*, 2007] and the early compressional stage during the Late Cretaceous. Fortunately, this compression probably altered the initial geometry to a limited extent because of the low angle of the unconformity underlying the Upper Albian sandstones, which can be found in several areas of the Cameros Basin and the Iberian Range [*Muñoz et al.*, 1997; *Salas et al.*, 2001].

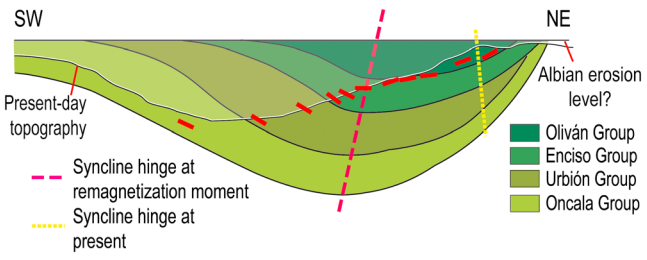

Figure 8. Sketch showing the obtained paleodips (short lines near the present-day topography) at the remagnetization time (not at scale).

Paleomagnetic data indicate that a significant part of the southern limb of the Northern Cameros Syncline, which forms at present a monoclinal panel, belonged to the southern limb of the preremagnetization syncline (Figure 9). On the other hand, the 5 km wide northernmost segment of this monocline shows paleomagnetic data consistent with the south dipping, northern limb of the preremagnetization syncline. Additionally, the

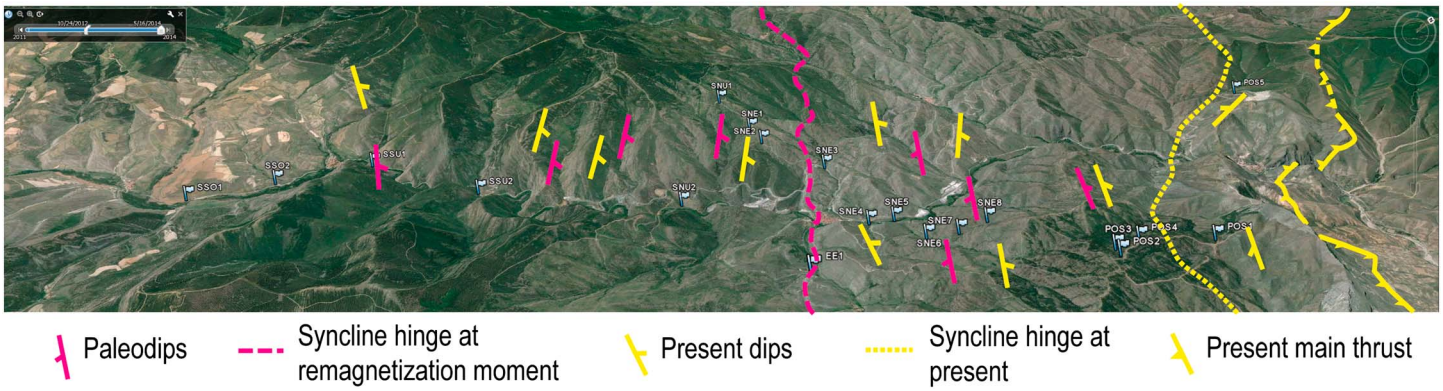

Figure 9. Aerial view of the Cidacos Valley (from Google Earth) in which we represent the considered paleomagnetic sites, the present dips of beds, paleodips at the remagnetization time, the present position of the syncline hinge, and the inferred position of this hinge at the remagnetization time.

northern limb of the present-day Northern Cameros Syncline shows paleomagnetic vectors consistent with bedding orientation obtained during the remagnetization event (Figures 9 and 10). However, some sites belonging to the Oliván Group would need a more complex (probably two stages) reconstruction since they involve late N-S trending folds. These noncoaxial orientations between extensional and compressional stages observed toward the basin border imply that bedding data should be carefully considered. Those oblique folds probably resulted from the adaptation of the synrift units to the geometry of the footwall during Cenozoic thrusting.

In the northern sector of the present-day Cameros monocline, paleomagnetic data suggest a 5 km migration of the Mesozoic syncline hinge, agreeing with the orientation of cleavage observed at discrete points (Figures 9 and 10). This large-scale hinge migration process requires a mechanism of kilometric scale. Basement-involved thrusts are often related to homogeneously dipping reverse faults that usually can be followed to significant depths [e.g., *Erslev*, 1993; *Erslev and Rogers*, 1993]. However, this kind of structures does not account for strong deformations and fold migration within the stratified series overlying the basement. On the opposite end-member of intraplate thrusting, the existence of a detachment level between basement and cover series can favor the independent movement of the latter [e.g., *Muñoz*, 1992; *Muñoz et al*., 1997; *Casas et al*., 2003], thus favoring the formation of buckle folds [*Simón*, 2004, 2005] or thrust-related folds [*Nebot and Guimerà*, 2016]. Within the Iberian Range, the geometry of previous structures, the changes in thickness of the Mesozoic sedimentary cover and the presence or absence of detachment levels yielded the coexistence of different tectonic styles [e.g., *Álvaro*, 1995; *Guimerà and Alvaro*, 1990; *Liesa et al*., 2006]. These mixed behaviors have been reported even within the same geological setting, as occurs in the Cameros unit [e.g., *Casas-Sainz*, 1993; *Casas-Sainz et al*., 2016].

In our case, the Upper Triassic Keuper units behave as a detachment level between the Paleozoic and the Jurassic-Cretaceous series and favor the independent movement of the Mesozoic cover with respect to the Paleozoic [*Casas et al*., 2009]. This separated movement is evident at the borders of the Cameros Massif, where the cover thrusts superimpose the supra-Triassic units of the Mesozoic Cameros Basin over the Almazán Cenozoic Basin to the south and the Ebro Basin to the north (Figure 2) [*Casas et al*., 2000]. Both thrusts contributed to the configuration of the Cameros inverted basin as a pop-up structure [*Guimerà et al*., 1995]. The southern thrust limiting the Cameros units is of particular relevance because it reveals a relative movement between the basement and the cover along the Upper Triassic décollement. It shows a 5 km relative displacement of the Cameros Basin toward the south over the Almazán Basin [*Platt*, 1990; *Guimerà et al*., 1995] that must be related with an equivalent northward movement of the Paleozoic basement along the main north verging Cameros Thrust. This northern thrust, when considering the basement, is the result, in its turn, of the compressional reactivation of a large normal fault with plurikilometric heave, almost totally recovered during shortening [e.g., *Casas-Sainz*, 1993]. Precisely, the southward movement of the Mesozoic cover at the southern basin border would be responsible for the large-scale hinge migration (Figures 9 and 10): in this case, this 5 km shortening associated with the reactivation of the normal fault in the basement brought about the transfer of displacement toward the south through the detachment level, instead of the

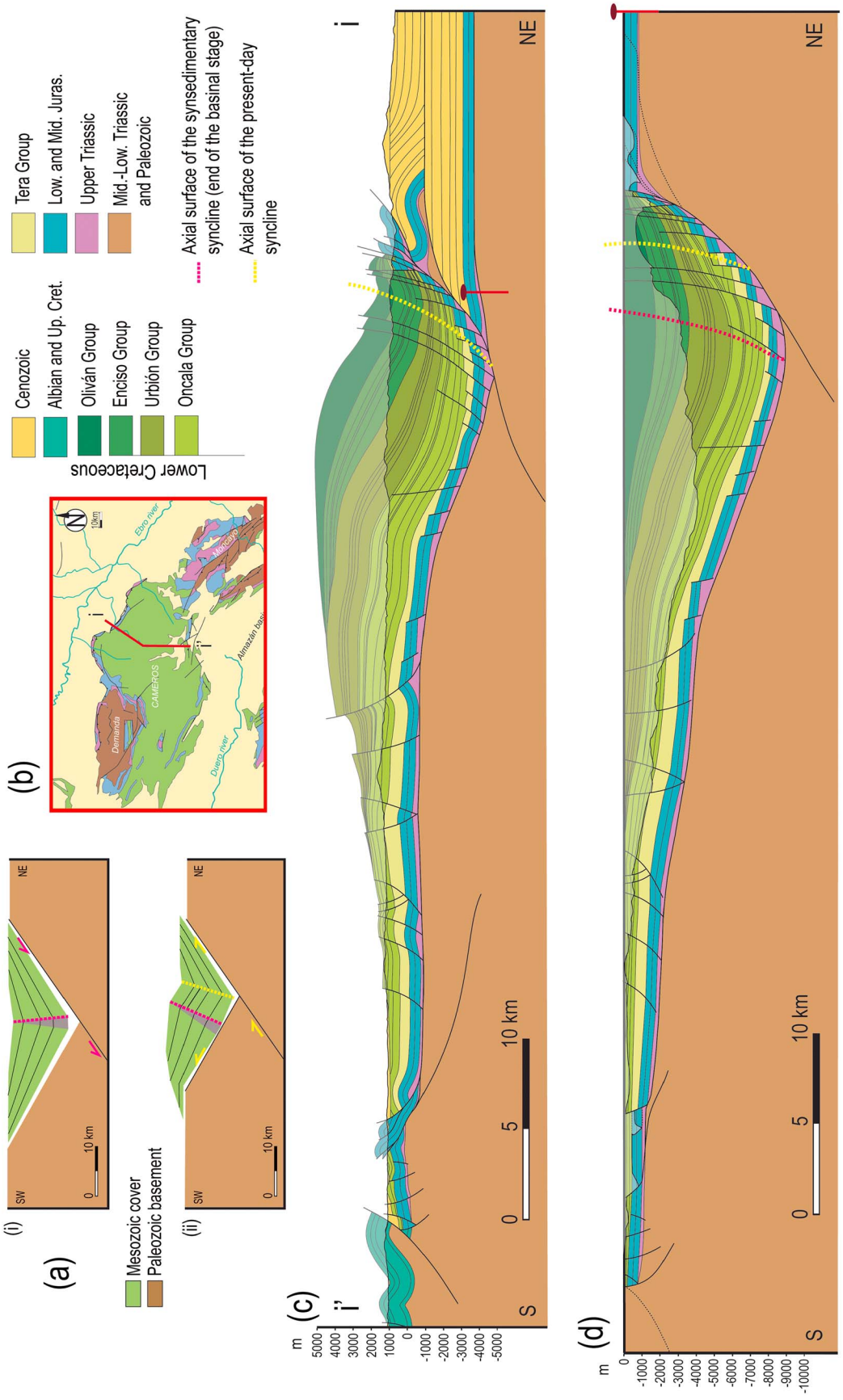

Figure 10. (a) Conceptual sketch showing the proposed mechanism for hinge migration in the Cameros basin (note that Cenozoic deposits are not considered). Not at scale. (b) Approximate location of the cross section. (c) Cross section of the eastern part of the Cameros basin along the Cidacos Valley and the Soria high plains. (d) Cross section restored to Albian times (end of basinal stage).

continuation of the northward movement, in agreement with models of hinge migration (see Figure 1). According to our paleomagnetic data, the amount of displacement in the southern border approximately equals the amount of hinge migration for the basin center during the Cenozoic tectonic inversion.

Therefore, our data allow us to (i) confirm a relationship between the Mesozoic cleavage and fold geometry before the Cenozoic inversion, as previously proposed by *Casas-Sainz and Gil-Imaz* [1998] and (ii) show that paleomagnetism may represent a tool to reconstruct folds geometry, provided that a widespread remagnetization between two significant moments in basin evolution occurred. The possibility to get a denser paleomagnetic data set with respect to cleavage analysis allows for better definition of fold hinges and a more accurate reconstruction of paleofold/basin geometry. Cleavage is discontinuous and constrained to particular rock types, especially in areas with very low to low metamorphic grade [*Gil Imaz*, 2001]. The use of remagnetizations would be feasible even in the absence of other deformational markers.

7. Conclusions

Paleomagnetic results from 20 sites collected along the Cidacos Valley (eastern part of the Cameros Basin, Northern Spain), together with the previous sites [*Villalaín et al*., 2003; *Casas et al*., 2009], confirm that the Lower Cretaceous series of the Cameros Basin underwent a normal polarity remagnetization event that can be bracketed between the Mesozoic extensional and the Cenozoic compressional stages. The remagnetized direction was isolated unequivocally in the Lower Cretaceous synrift series, confirming the widespread effect of the remagnetization, as both hematites in red beds and magnetite and pyrrhotite in limestones show that remagnetized component.

The SCI method was successfully applied to the remagnetized vectors obtained in the 20 sites of this study together with the 22 previous paleomagnetic sites from *Villalaín et al*. [2003], located in a close area of the Cameros Basin. The direction of the remagnetized paleomagnetic vector according to this method is as follows: Dec. = 350.4° and Inc. = 53.2°.

The existence of this (preinversion) remagnetization allowed us to apply the asymmetric solution method to the 20 sites sampled in this study to finally reconstruct the extensional geometry of the northern border of the Cameros Basin at the remagnetization time. This procedure corroborates a synclinal geometry for the thick synrift series during Cretaceous times.

Bedding restoration reveals two main groups of sites according to their paleo-attitude, indicating their position in the northern or southern limb of a large-scale syncline (that differs from the present day fold) during the remagnetization time. Sites located southwestward show a northward paleodip at the remagnetization time, whereas in sites located northeastward, strata had a south dipping original attitude opposite to their current dip. The limit between the two groups of sites can be accurately positioned by means of paleomagnetic dat, and is interpreted to separate the two limbs of the paleosyncline. A northeastward migration of around 5 km of the axial surface of the basin-scale Northern Cameros Syncline can be inferred, associated with the Cenozoic Basin inversion.

Acknowledgments

We acknowledge T. Román-Berdiel for her inestimable help during the development of this study. We also thank the helpful assistance of Leonardo Sagnotti and Aldo Winkley during the paleomagnetic measurements at the INGV and P. Calvin for his help to perform the regional fold test. The thorough revisions from two external referees helped to improve substantially the quality of this article. This research was financed by the research project CGL2009-08969 of the MICINN (Spanish Ministry of Science and Innovation) and the research projects CGL2012-38481, CGL2013- 42670-P, and CGL2016-77560 of the MINECO (Spanish Ministry of Economy and Competitiveness) with also FEDER founding (European Union). C. García-Lasanta acknowledges a research grant of the Institute of Riojan Studies and the grant BES-2010-037509 of the MICINN. Raw paleomagnetic data, field pictures and enlarged maps, and cross sections are available from the authors upon request (cgarcialasanta@gmail.com, acasas@unizar.es, villa@ubu.es).

References

Álvaro, M. (1995), La Cadena Ibérica, in *XXIX Curso de Geología Práctica*, edited by A. Meléndez and M. Gutiérrez, pp. 1–28, Universidad de Zaragoza, Teruel, Spain.

Aubourg, C., J. P. Pozzi, and M. Kars (2012), Burial, claystones remagnetization and some consequence for magnetostratigraphy, in *Remagnetization and Chemical Alteration of Sedimentary Rocks*, *Special Publication 371*, edited by R. D. Elmore, pp. 181–188, Geological Society, London.

Banerjee, S., R. D. Elmore, and M. H. Engel (1997), Chemical remagnetization and burial diagenesis: Testing the hypothesis in the Pennsylvanian Belden Formation, Colorado, *J. Geophys. Res.*, *102*, 24,825–24,842, doi:10.1029/97JB01893.

Blumstein, A. M., R. D. Elmore, M. H. Engel, C. Elliot, and A. Basu (2004), Paleomagnetic dating of burial diagenesis in Mississippian carbonates, Utah, *J. Geophys. Res.*, *109*, B04101, doi:10.1029/2003JB002698.

Buchanan, P. G., and K. R. McClay (1991), Sandbox experiments of inverted listric and planar fault systems, *Tectonophysics*, *188*(1–2), 97–115.

Butler, R. W. H. (1992), Thrust zone kinematics in a basement-cover imbricate stack; eastern Pelvoux massif, French Alps, *J. Struct. Geol.*, *14*(1), 29–40.

Casas, A. M., A. L. Cortés-Gracia, and A. Maestro-González (2000), Intra-plate deformation and basin formation during the Tertiary within the Northern Iberian plate: Origin and evolution of the Almazán Basin, *Tectonics*, *19*, 258–289, doi:10.1029/1999TC900059.

Casas, A. M., B. Oliva, T. Román-Berdiel, and E. Pueyo (2003), Basement deformation: Tertiary folding and fracturing of the Variscan Bielsa granite (axial zone, central Pyrenees), *Geodin. Acta*, *16*, 99–117.

Casas, A. M., J. J. Villalaín, R. Soto, A. Gil-Imaz, P. Del Río, and G. Fernández (2009), Multidisciplinary approach to an extensional syncline model for the Mesozoic Cameros Basin (N Spain), *Tectonophysics*, *470*, 3–20.

Casas-Sainz, A. M. (1991), El frente norte de las Sierras de Cameros: Estructuras cabalgantes y campo de esfuerzos, PhD thesis Universidad de Zaragoza. Zubía, Monográfico 4, Instituto de Estudios Riojanos.
Casas-Sainz, A. M. (1993), Oblique tectonic inversion and basement thrusting in the Cameros Massif (Northern Spain), *Geodin. Acta*, *6*(3), 202–216.
Casas-Sainz, A. M., and C. Faccenna (2001), Tertiary compressional deformation of the Iberian plate, *Terra Nova*, *13*, 281–288.
Casas-Sainz, A. M., and A. Gil-Imaz (1998), Extensional subsidence, contractional holding and thrust inversion of the eastern Cameros Basin, northern Spain, *Int. J. Earth Sci. (Geologische Rundschau)*, *86*, 802–818.
Casas-Sainz, A. M., T. Román-Berdiel, B. Oliva-Urcia, C. García-Lasanta, J. J. Villalaín, L. Aldega, S. Corrado, C. Caricchi, C. Invernizzi, and M. C. Osácar (2016), Multidisciplinary approach to constrain kinematics of fault zones at shallow depths: A case study from the Cameros-Demanda thrust (North Spain), *Int. J. Earth Sci. (Geol Rundsch)*, doi:10.1007/s00531-016-1349-5.
Casquet, A., C. Galindo, J. M. González-Casado, A. Alonso, R. Mas, M. Rodas, E. García, and J. F. Barrenechea (1992), El metamorfismo en la cuenca de los Cameros. Geocronología e implicaciones tectónicas, *Geogaceta*, *11*, 22–25.
Chadima, M., and F. Hrouda (2006), Remasoft 3.0: A user-friendly paleomagnetic data browser and analyzer, *Trav. Géophys.*, *27*, 20–21.
Del Río, P., L. Barbero, P. Mata, and C. M. Fanning (2009), Timing of diagenesis and very low-grade metamorphism in the eastern sector of the Sierra de Cameros (Iberian range, Spain): A U–Pb SHRIMP study on monazite, *Terranova*, *21*, 438–445.
Elmore, R. D., A. R. Muxworthy, and M. Aldana (2012), Remagnetization and chemical alteration of sedimentary rocks, *Geol. Soc. London Spec. Publ.*, *371*(1), 1–21.
Erslev, E. A. (1993), Thrusts, back-thrusts, and detachment of Laramide foreland arches, in *Laramide Basement Deformation in the Rocky Mountain Foreland of the Western United States*, *Geol. Soc. Am. Spe. Pap.*, vol. 280, edited by C. J. Schmidt, R. Chase, and E. A. Erslev, pp. 339–358.
Erslev, E. A., and J. L. Rogers (1993), Basement-cover geometry of Laramide fault-propagation folds, in *Laramide Basement Deformation in the Rocky Mountain Foreland of the Western United States*, *Geol. Soc. Am. Spe. Pap.*, vol. 280, edited by C. J. Schmidt, R. Chase, and E. A. Erslev, pp. 125–146.
Fisher, R. A. (1953), Dispersion on a sphere, in *Proceedings of the Royal Society of London*, *Series A*, vol. 217, pp. 295–305, The Royal Society.
Galdeano, A., M. G. Moreau, J. P. Pozzi, P. Y. Berthou, and J. A. Malod (1989), New paleomagnetic results from Cretaceous sediments near Lisboa (Portugal) and implications for the rotation of Iberia, *Earth Planet. Sci. Lett.*, *92*, 95–106.
García-Lasanta, C., B. Oliva-Urcia, T. Román-Berdiel, A. M. Casas, and A. M. Hirt (2014), Understanding the Mesozoic kinematic evolution in the Cameros basin (Iberian Range, NE Spain) from magnetic subfabrics and mesostructures, *J. Struct. Geol.*, *66*, 84–101.
GEODE (2014), Sistema de Información Geológica Continua: SIGECO, IGME. J. Navas (ed.) (reference date 18/07/2014). [Available at http://cuarzo.igme.es/sigeco/default.htm.]
Gil Imaz, A. (2001), La estructura de la Sierra de Cameros: Deformación dúctil y su significado a escala cortical, Instituto de Estudios Riojanos, Ciencias de la Tierra, 23, 301 pp.
Goldberg, J. M., M. Guiraud, H. Maluski, and M. Séguret (1988), Caractères pétrologiques et âge du métamorphisme en contexte distensif du bassin sur décrochement de Soria (Crétacé inférieur, Nord Espagne), *Comptes rendus de l'Acad. Sci., París*, *307*, 521–527.
Guimerà, J., A. Alonso, and R. Mas (1995), Inversion of an extensional-ramp basin by a newly formed thrust: The Cameros Basin (N Spain), in *Basin Inversion*, *Geol. Soc., London Spec. Publ.*, vol. 88, edited by J. G. Buchanan and P. G. Buchanan, pp. 433–453.
Guimerà, J., and M. Álvaro (1990), Structure et évolution de la compression alpine dans la Chaîne Ibérique et la Chaîne côtière catalane (Espagne), *Bull. Soc. Géol. Fr.*, *6*(2), 339–348.
Guiraud, M. (1983), Evolution tectono-sédimentaire du bassin wealdien (Crétacé inferieur) en relais de décrochements de Logroño-Soria (NW Espagne), Thèse de III cycle, Univ. des Sciences et Techniques du Languedoc.
Guiraud, M., and M. Séguret (1985), Releasing solitary overstep model for the Late Jurassic-Early Cretaceous (Wealdian) Soria strike-slip basin (North Spain), in *In Strike-Slip Deformation, Basin Formation and Sedimentation*, *Soc. Econ. Paleon. Mineral., Special Plublication*, vol. 37, edited by K. T. Biddle and N. Christie-Blick, pp. 159–175.
Henry, B., H. Rouvier, and M. Le Goff (2004), Using syntectonic remagnetizations for fold geometry and vertical axis rotation: The example of the Cevennes border (France), *Geophys. J. Int.*, *157*, 1061–1070.
Jamison, W. R. (1987), Geometrical analysis of fold development in overthrust terranes, *J. Struct. Geol.*, *9*(2), 207–219.
Katz, B., R. D. Elmore, M. Cogoini, and S. Ferry (1998), Widespread chemical remagnetization: Orogenic fluids or burial diagenesis of clays, *Geology*, *26*, 603–606.
Liesa, C. L., A. R. Soria, N. Meléndez, and A. Meléndez (2006), Extensional fault control on the sedimentation patterns in a continental rift basin: El Castellar Formation, Galve sub-basin, Spain, *J. Geol. Soc.*, *163*, 487–498.
Lowrie, W. (1990), Identification of ferromagnetic minerals in a rock by coercivity and unblocking temperature properties, *Geophys. Res. Lett.*, *17*, 159–162, doi:10.1029/GL017i002p00159.
Mata, M. P. (1997), Caracterización y evolución mineralógica de la cuenca mesozoica de Cameros (Soria-La Rioja), PhD thesis, Universidad de Zaragoza.
Mata, M. P., A. M. Casas, A. Canals, A. Gil, and A. Pocoví (2001), Thermal history during Mesozoic extension and tertiary uplift in the Cameros Basin, Northern Spain, *Basin Res.*, *13*, 91–111.
McCaig, A. M., and E. McClelland (1992), Palaeomagnetic techniques applied to thrust belts, in *Thrust Tectonics*, edited by K. R. McClay, pp. 209–216, Chapman and Hall, London.
McClay, K. R. (1989), Analogue models of inversion tectonics, in *Geological Inversion Tectonics Meeting*, *Geol. Soc. London Spec. Publ.*, vol. 44, edited by M. A. Cooper and G. D. Williams, pp. 41–59.
McClay, K. R. (1995), The geometries and kinematics of inverted fault systems: A review of analogue model studies, in *Basin Inversion*, *Geol. Soc. London Spec. Publ.*, vol. 88, edited by J. G. Buchanan and P. G. Buchanan, pp. 97–118.
McClelland, E., V. Courtillot, and P. E. Tapponier (Eds.) (1986), Magnetotectonics – Introduction, *Tectonics*, *5*(5), 709–711.
Mercier, E., S. Rafini, and R. Ahmadi (2007), Fold kinematics in "fold-and-thrust belts". The 'hinge migration' question, a review, in *Thrust Belts and Foreland Basins. From Fold Kinematics to Hydrocarbon Systems, Chapter 7*, *Frontiers in Earth Sciences*, pp. 135–147, Springer, Berlin/Heidelberg.
Mitra, S. (1990), Fault-propagation folds: Geometry, kinematic evolution and hydrocarbon traps, *Am. Assoc. Pet. Geol. Bull.*, *74*, 921–945.
Moreau, M. G., J. Y. Berthou, and J. A. Malod (1997), New paleomagnetic Mesozoic data from the Algarve (Portugal): Fast rotation of Iberia between the Hauterivian and the Aptian, *Earth Planet. Sci. Lett.*, *146*, 689–701.
Mueller, K., and J. Suppe (1997), Growth of wheeler ridge anticline, California: Geomorphic evidence for fault-bend folding behaviour during earthquakes, *J. Struct. Geol.*, *19*(3–4), 383–396.
Muñoz, J. A. (1992), Evolution of continental collision belt: ECORS-Pyrenees crustal balanced cross-section, in *Thrust Tectonics*, edited by K. McClay, pp. 235–246, Chapman and Hall, London.

Muñoz, J. A., P. Coney, K. McClay, and C. Evenchick (1997), Discussion on syntectonic burial and post-tectonic exhumation of the southern Pyrenees foreland fold-thrust belt, *J. Geol. Soc. London*, *154*, 361–365.
Nebot, M., and J. Guimerà (2016), Structure of an inverted basin from subsurface and field data: The late Jurassic-early Cretaceous Maestrat Basin (Iberian chain), *Geol. Acta*, *14*, 155–179.
Neres, M., E. Font, J. M. Miranda, P. Camps, P. Terrinha, and J. Mirao (2012), Reconciling Cretaceous paleomagnetic and marine magnetic data for Iberia: New Iberian paleomagnetic poles, *J. Geophys. Res.*, *117*, B06102, doi:10.1029/2011JB009067.
Neres, M., J. M. Miranda, and E. Font (2013), Testing Iberian kinematics at Jurassic-Cretaceous times, *Tectonics*, *32*, 1312–1319, doi:10.1002/tect.20074.
Platt, N. (1990), Basin evolution and fault reactivation in the western Cameros Basin, Northern Spain, *J. Geol. Soc. London*, *147*, 165–175.
Salas, R., J. Guimerà, R. Mas, C. Martín-Closas, A. Meléndez, and A. Alonso (2001), Evolution of the Mesozoic central Iberian rift system and its Cainozoic inversion (Iberian chain), in *Peri-Tethyd Memoir 6: Peri-Tethyan Rift/Wrench Basins and Passive Margins*, vol. 186, edited by P. A. Ziegler et al., pp. 145–185, Mémoirs Museum National dHistoire Naturelle, Paris.
Shipunov, S. V. (1997), Synfolding magnetization: Detection, testing and geological applications, *Geophys. J. Int.*, *130*, 405–410.
Simón, J. L. (2004), Superposed buckle folding in the eastern Iberian Chain, Spain, *J. Struct. Geol.*, *26*(8), 1447–1464.
Simón, J. L. (2005), Erosion-controlled geometry of buckle fold interference, *Geology*, *33*(7), 561–564.
Soto, R., A. M. Casas-Sainz, J. J. Villalaín, and B. Oliva-Urcia (2007), Mesozoic extension in the Basque-Cantabrian basin (N Spain). Contributions from AMS and brittle mesostructures, *Tectonophysics*, *445*, 373–394.
Soto, R., A. M. Casas-Sainz, and J. J. Villalaín (2011), Widespread Cretaceous inversion event in the northern Spain: Evidence from subsurface and paleomagnetic data, *J. Geol. Soc. London*, *168*, 899–912.
Soto, R., J. J. Villalaín, and A. M. Casas-Sainz (2008), Remagnetizations as a tool to analyze the tectonic history of inverted sedimentary basins: A case study from the Basque-Cantabrian basin (north Spain), *Tectonics*, *27*, TC1017, doi:10.1029/2007TC002208.
Storetvedt, K. M., H. Mogstad, M. C. Abranches, J. G. Mitchell, and A. Serralheiro (1987), Paleomagnetism and isotopic age data from upper Cretaceous igneous rocks of W. Portugal, geological correlation and plate tectonic aspects, *Geophys. J. R. Astron. Soc.*, *88*(1), 241–263.
Suppe, J. (1983), Geometry and kinematics of fault-bend folding, *Am. J. Sci.*, *283*, 684–721.
Tauxe, L. (1998), *Paleomagnetic Principles and Practise*, *Modern Approaches in Geophysics*, vol. 17, Kluwer Acad., London.
Tauxe, L. (2010), *Essentials of Paleomagnetism*, Appendix F. Computer Skills., Univ. of California Press, Berkeley.
Tischer, G. (1966), El delta Wealdico de las montañas Ibéricas Occidentales y sus enlaces tectónicos, Notas y Comentarios, *Ins. Geol. Min. Esp.*, *81*, 53–78.
Tohver, E., A. B. Weil, J. G. Solum, and C. M. Hall (2008), Direct dating of chemical remagnetizations in sedimentary rocks, insights from clay mineralogy and 40Ar/39Ar age analysis, *Earth Planet. Sci. Lett.*, *274*, 524–530.
Torres-López, S., J. J. Villalaín, A. M. Casas, H. El Ouardi, B. Moussaid, and V. C. Ruiz-Martínez (2014), Widespread Cretaceous secondary magnetization in the High Atlas (Morocco). A common origin for the Cretaceous remagnetizations in the western Tethys?, *J. Geol. Soc. London*, *23*(4), 2013–2107.
Van der Voo, R. (1969), Paleomagnetic evidence for the rotation of the Iberian Peninsula, *Tectonophysics*, *7*, 5–56.
Van der Voo, R. (1990), The reliability of paleomagnetic data, *Tectonophysics*, *184*, 1–9.
Van der Voo, R. (1993), *Paleomagnetism of the Atlantic, Tethys and Iapetus Oceans*, p. 441, Cambridge Univ. Press, Cambridge.
Van der Voo, R., and T. H. Torsvik (2012), The history of remagnetization of sedimentary rocks: Deceptions, developments and discoveries, in *Remagnetization and Chemical Alteration of Sedimentary Rocks*, *Geol. Soc., London Spec. Publ.*, vol. 371, edited by R. D. Elmore et al., pp. 23–53.
Villalaín, J. J., G. Fernández-González, A. M. Casas, and A. M. Gil-Imaz (2003), Evidence of a Cretaceous remagnetization in the Cameros Basin (North Spain). Implications for basin geometry, *Tectonophysics*, *377*, 101–117.
Villalaín, J. J., A. Casas-Sainz, R. Soto, and S. Torres-López (2012), The widespread Cretaceous remagnetizations in Mesozoic intraplate basins from Iberia and North Africa. Contribution to tectonic studies, *Contrib. Geophys. Geodesy*, *42*, 121–122.
Villalaín, J. J., A. Casas-Sainz, and R. Soto (2015), Reconstruction of inverted sedimentary basins from syn-tectonic remagnetizations. A methodological proposal, in *Palaeomagnetism in Fold and Thrust Belts: New Perspectives*, *Geol. Soc., London Spec. Publ.*, vol. 425, edited by E. L. Pueyo et al., pp. 233–246, doi:10.1144/SP425.10.
Waldhör, M., and E. Appel (2006), Intersections of remanence small circles: New tools to improve data processing and interpretation in palaeomagnetism, *Geophys. J. Int.*, *166*, 33–45.
Watson, G. S., and R. J. Enkin (1993), The fold test in paleomagnetism as a parameter estimation problem, *Geophys. Res. Lett.*, *20*, 2135–2137, doi:10.1029/93GL01901.
Weil, A. B., and A. J. Sussman (2004), Classifying curved orogens based on timing relationships between structural development and vertical-axis rotations, *Geol. Soc. Am. Spec. Pap.*, *383*, 1–15.
Ziegler, P. A. (1988), Evolution of the Arctic-North Atlantic and the Western Tethys. American Association of Petroleum Geologists, *Memoir*, *43*, 198.
Zijderveld, J. D. A. (1967), A.C. Demagnetization of rocks: Analysis of results, in *Methods in Paleomagnetism*, edited by D. W. Collinson, S. K. Runcorn, and K. M. Creer, pp. 254–286, Elsevier, New York.